Available online at www.sciencedirect.com
SCIENCE DIRECT®
Journal of Nuclear Materials 337–339 (2005) 139–145
journal of nuclear materials
www.elsevier.com/locate/jnucmat

OSM-EIRENE modeling of neutral pressures in the Alcator C-Mod divertor

S. Lisgo [a,*], P. Börner [c], C. Boswell [b], D. Elder [a], B. LaBombard [b], B. Lipschultz [b], C.S. Pitcher [a], D. Reiter [c], P.C. Stangeby [a], J.L. Terry [b], S. Wiesen [c]

[a] University of Toronto Institute for Aerospace Studies, Toronto, Canada M3H 5T6
[b] MIT Plasma Science and Fusion Center, Cambridge, MA 02139, USA
[c] IPP, Forschungszentrum Juelich GmbH, EURATOM Association, D-52425 Juelich, Germany

Abstract

The ITER divertor will be more collisional than divertors in existing tokamaks and the neutral modeling tools used for predictive ITER modeling need to be validated for similar divertor conditions in order to increase confidence in the results. The EIRENE neutral code has been applied to the Alcator C-Mod divertor, where collisional effects such as Lyman series photon trapping and neutral viscosity have been observed. The plasma solution used as input to EIRENE agrees well with the available diagnostic data for the divertor and was generated using an empirical Onion-Skin Method interpretive code that requires a large amount of experimental data as input. The calculated divertor pressure is 11 ± 3 mTorr, a factor ~ 2 lower than the measured value of 25 ± 3 mTorr. The neutral solution is sensitive to photon trapping, viscosity, elastic collisions between plasma ions and molecules, and the amount of leakage through the outer divertor substructure.

PACS: 52.55; 52.20.H; 52.65
Keywords: Alcator C-Mod; Divertor modelling; OSM; EIRENE; Neutrals

1. Introduction

The ITER divertor will have shorter neutral mean free path lengths scaled to machine size than the current generation of tokamaks, resulting in more strongly coupled neutral, ion and photon populations. It is well known that neutral dynamics are an important component of edge physics [1] and are central to several ITER-critical issues such as detachment, pumping, impurities, and (perhaps) access to H-mode. Also, the strong absorption of Lyman series photons by atoms can significantly affect ionisation profiles [2]. Sophisticated kinetic Monte-Carlo neutral codes such as EIRENE [3] and DEGAS2 [4] are available for investigating these neutral interactions, but are typically applied assuming free-molecular transport and optical transparency.

* Corresponding author. Address: D3/2.15, Fusion Association, Culham Science Center, Abingdon, Oxfordshire OX14 3DB, UK. Tel.: +011 44 1235 466619; fax: +011 44 1235 466379.
E-mail address: steven@starfire.utias.utoronto.ca (S. Lisgo).

0022-3115/$ - see front matter © 2004 Elsevier B.V. All rights reserved.
doi:10.1016/j.jnucmat.2004.09.073

Alcator C-Mod [5] is a high magnetic field (up to 9 T) divertor tokamak that currently represents the best opportunity to validate neutral codes for ITER-like divertor conditions, a requirement for increased confidence in predictive modeling studies for ITER. Measured neutral pressures in the C-Mod divertor approach 100 mTorr, indicating the presence of neutral viscosity [6], and there have also been observations of strong Lyman α (Ly_α) photon trapping [2]. However, two initial efforts to calculate the divertor neutral pressure with DEGAS2 gave results a factor ~10 lower than the measured value. The first attempt employed a rather simple plasma solution [7] as input to DEGAS2 and therefore a large discrepancy is not surprising, but the subsequent plasma solution was more detailed and was generally consistent with a significant amount of spectroscopic data [8]. It has been suggested that inaccuracies in the plasma solutions contributed significantly to the pressure discrepancies [9].

The objectives of the present study are: (a) use improved interpretive methods and the full experimental data set available for the C-Mod divertor to produce a 'reasonably accurate' and detailed description of the divertor plasma, and then (b) *quantitatively* assess the sensitivity of the neutral solution to the neutral physics in EIRENE. A more complete account of the results presented here can be found in Ref. [10].

2. Generation of the divertor plasma solution

EIRENE requires 2D distributions of the electron temperature, T_e, and plasma density, n_e, as input (assuming toroidal symmetry and $T_i = T_e$). The standard edge 2D fluid codes are most commonly used to specify the T_e and n_e profiles, but an interpretive method termed 'plasma reconstruction' that relies extensively on experimental data is utilized in the present work. Discharge 990429019 at 950 ms is modeled, with $I_p = 0.8$ MA, $\bar{n}_e = 1.46 \times 10^{20}$ m^{-3} $= 0.3 n_{GW}$, $B_T = 5.4$ T, deuterium majority, lower single-null, and $B \times \nabla B$ towards the divertor; the same shot that was used for the previous efforts to model the divertor pressure with DEGAS2. A review of the diagnostic data indicates partial detachment in the inner divertor and outer PFZ, where $T_e \approx 1$ eV and $n_e \approx 10^{21}$ m^{-3}; see Section 2.2. Volume recombination is very sensitive to T_e and n_e for these plasma conditions [11] which suggests that the divertor neutral solution is strongly dependant on the T_e and n_e profiles input to EIRENE. The low T_e values also imply neutral ionization/dissociation mean free paths on the order of the geometric scale length, so that a detailed plasma solution is required for the entire divertor, not just near the gas box where the pressure measurement is made. The plasma in the outer SOL is attached.

2.1. Empirical reconstruction of the detached plasma profiles

The plasma solution is generated by the OSM code which employs the Onion-Skin Method [12]. The boundary conditions are specified in the divertor and the full 2D solution is assembled from a series of nested solutions for individual flux-tubes. $T_i = T_e$ is assumed, which is a reasonable approximation given the short e-i equilibration times in the C-Mod divertor.

The interpretive method used to generate the detached plasma profiles is detailed elsewhere [10,13]. In brief, a simple parameterized model of detachment is used as a template for parallel T_e and n_e variations in detached plasma; the parameters are set from comparisons with probe and spectroscopic measurements. The validity of the resulting T_e, n_e distributions depends on the level of agreement with the full experiment data set and on having sufficient data available to constrain the solution.

The standard OSM 1D fluid model [14] (based on conservation equations) is applied for the attached plasma in the outer SOL and upstream of the detached region in the inner SOL.

2.2. Comparison with the available experimental data for the divertor

Considerable experimental effort has been made to measure the plasma conditions in the C-Mod divertor; see Fig. 1.

The divertor pressure is measured at the bottom of a 1.26 m vertical access port which descends from the floor of the gas box (referred to here as 'the plenum') located behind the outer target. The measured value, p_{div}^{expt}, is 25 ± 3 mTorr with the uncertainty from the scatter in the pressure data for shots with similar $\bar{n}_e$ and from the same run day as the modeled shot.

Langmuir probe arrays are embedded in the inner and outer target plates [16]. The probe T_e data for the inner divertor are shown in Fig. 2(a) and the data points above the inner nose are much higher than T_e values estimated from Balmer line ratios; see Fig. 4(a) for $\theta < 161°$. The difficulty interpreting these Langmuir probe characteristics is consistent with similar comparisons on other tokamaks [17] and Langmuir probe T_e data are generally considered unreliable below ~5 eV. Therefore, the model T_e boundary conditions for the inner divertor are set based on agreement with spectroscopic data, although note that the probes below the inner nose are in reasonable agreement with the model values. The I_{sat} measurements are applied as boundary conditions; see Fig. 2(b). There are no I_{sat} data for much of the inner PFZ but the D_γ emission profiles there (see Fig. 5(a)) are characteristic of strongly detached plasma and so nominal I_{sat} values are assigned. Fig. 2(e) shows substantial pressure loss between the inner target and

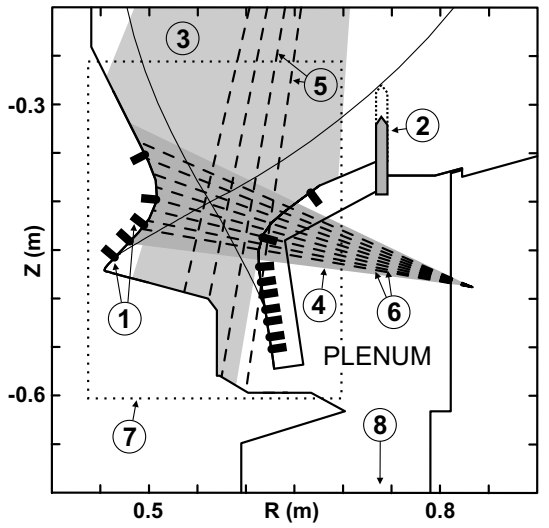

Fig. 1. Poloidal cross-section of the C-Mod divertor showing the available diagnostics: (1) target Langmuir probe arrays, (2) vertical reciprocating probe, (3) top-view photodiode array (D_α, shaded), (4) side-view photodiode array (D_α, shaded), (5) top-view spectrometer chords, (6) side-view spectrometer chords, (7) inversion region for a toroidally viewing CCD camera, and (8) pressure gauge.

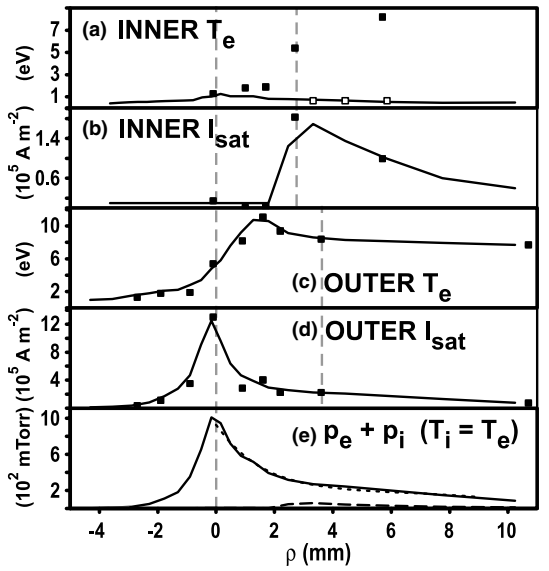

Fig. 2. (a)–(d) Target Langmuir probe data [B. LaBombard] (solid squares) compared to plasma model boundary conditions (lines). In (a), spectroscopic near-target T_e data is included (open squares) [B. Lipschultz]. (e) Outer target (solid), inner target (dashed) and upstream plasma pressure (dotted, from reciprocating probe). The vertical lines indicate the locations of the strike-points and the inner and outer divertor noses.

the upstream reciprocating probe, consistent with detachment. Conversely, the outer SOL probe data shown in Fig. 2(c)–(e) are typical of attached conditions. The probe T_e values drop to ~1 eV in the outer PFZ, in agreement with the spectroscopic data; see Fig. 3(a) for $\theta = 260.5°$. The apparent reliability of the outer divertor Langmuir probes for low T_e is unexplained at present.

The top- and side-view spectrometer and diode array data are compared with the model in Figs. 3 and 4, respectively. The temperature data, $T_{e,Saha}$, is calculated by fitting the measured emission ratios of the $p = 6, 7, 8, 9 \rightarrow 2$ Balmer lines to the Saha equation [15]. Stark broadening analysis [15] of these lines also gives an estimate of the electron density, $n_{e,Stark}$. These data are representative of (detached) plasma that is recombining in the volume since atomic excitation by electron impact does not efficiently populate these higher Balmer lines. There is general agreement with the $T_{e,Saha}$ and $n_{e,Stark}$ data, although the model is just outside the stated uncertainty in some cases. The $T_{e,Saha} = 0.5$ eV data point above the outer nose is due to light reflections [18], which are included in the simulation of the diagnostic. The high resolution diode arrays were equipped with a D_α filter and the model matches the shape of the measured profiles well but is higher in magnitude by a factor ~ 2.

The D_γ distribution from the inversion of the toroidally viewing camera is shown in Fig. 5(a). The model result in Fig. 5(b) matches the large features of the spatial distribution, but as with D_α, the calculated values are higher by a factor ~2. These discrepancies may be due to underestimates of the uncertainty in the experimental data or inaccuracies in the atomic physics. Note that modifying the plasma solution to reduce the

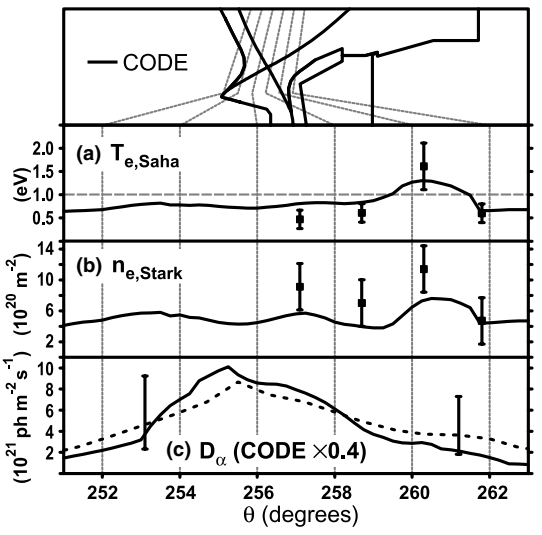

Fig. 3. Top-view spectroscopic data [(c) J. L. Terry]. See text for notes. The error bars in (c) are estimates for the experimental data.

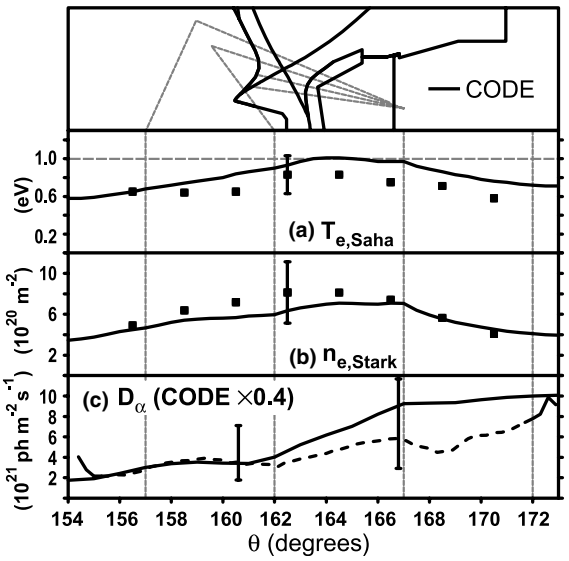

Fig. 4. Side-view spectroscopic data.

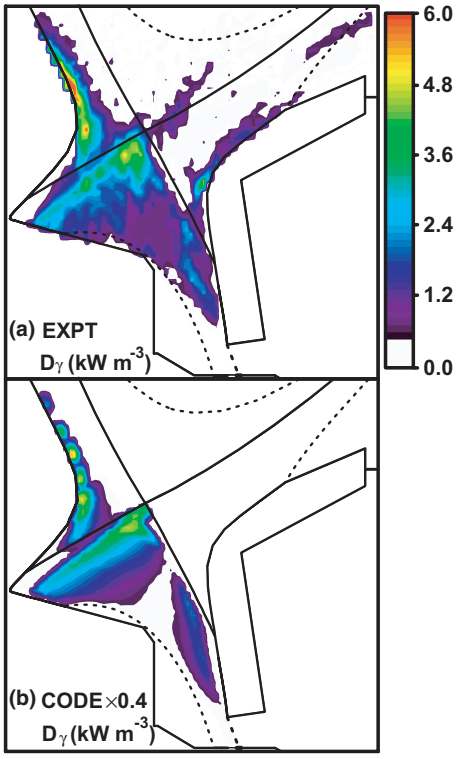

Fig. 5. Comparison of (a) experimental [C. Boswell] and (b) code D_γ profiles (linear scale).

calculated D_α and D_γ emissions results in clear disagreement with the $T_{e,Saha}$ and $n_{e,Stark}$ data; the D_α and D_γ results presented here give the best *overall* agreement with the full spectroscopic data set.

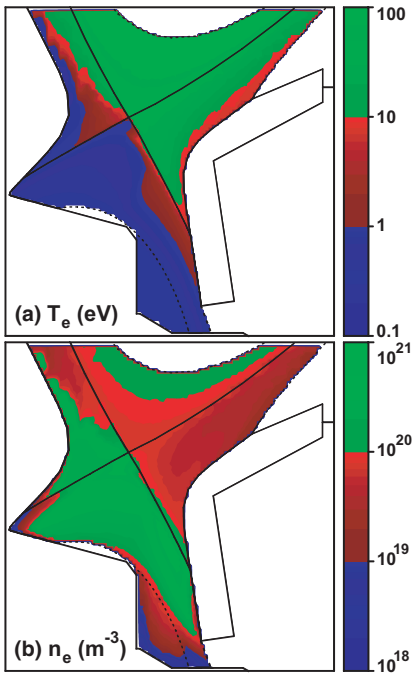

Fig. 6. Divertor plasma solution input to EIRENE (log scales).

Comparison with the reciprocating probe data is beyond the scope of this monograph and is presented in Ref. [10].

2.3. Plasma solution

The plasma solution is plotted in Fig. 6. T_e in the PFZ is highest near the outer leg of the separatrix and decreases to ~0.5 eV in the lower divertor. The plasma density peaks at $\sim 10^{21}$ m^{-3} near the x-point and near the separatrix in the outer PFZ. Given the broad agreement with the experimental data, it is hypothesized that the plasma solution is sufficiently accurate for investigating neutral dynamics in the C-Mod divertor.

3. Neutral modeling results and discussion

The divertor pressure calculated by EIRENE, p_{div}^{code}, is 17 ± 2 mTorr for the T_e and n_e profiles in Fig. 6. The error estimate is based on known uncertainties in the neutral model [10]. Agreement with $p_{div}^{expt} = 25 \pm 3$ mTorr is significantly improved compared to the previous neutral modeling studies for the C-Mod divertor [7,9]. The absolute error in the calculated pressure is representative of uncertainties in the neutral collision models in EIRENE.

Fig. 7(a) plots the source strengths for the listed divertor regions (the divertor is defined as the vertical target region below a line connecting the inner and outer 'noses'). The total volume recombination source, S_{rec}, is 1.7×10^{22} s^{-1}, which is on the same order as values from direct analysis of the $T_{e,Saha}$ and $n_{e,Stark}$ data [15] and 40% more than the total ion target flux of 1.2×10^{22} s^{-1}. Note that the *effective* volume recombination source is presented here; see Section 3.1.

The contribution of each neutral source to p_{div}^{code} is shown in Fig. 7(b). The outer PFZ target flux produces nearly half of the divertor pressure due to its close proximity to the plenum entrance, and despite having only ~1/3 the source strength of volume recombination in the PFZ. Almost all of the neutrals produced in the SOL are pumped by the plasma before entering the plenum.

The dependence of p_{div}^{code} on individual neutral processes is determined by removing each process in turn and recalculating the pressure; see Fig. 8. The neutral solution is most sensitive to Ly_α trapping, viscosity, and elastic collisions between plasma ions and neutral molecules, which are discussed in Sections 3.1–3.3.

It is important to acknowledge that the above results are for a 'sealed plenum' approximation where the *only* neutral leakage pathway between the plenum and the main chamber is through the divertor throat (the same assumption was made in the previous studies divertor studies [7,9]). The decrease in p_{div}^{code} after including a more realistic representation of the outer divertor structure in the model is discussed in Section 3.4.

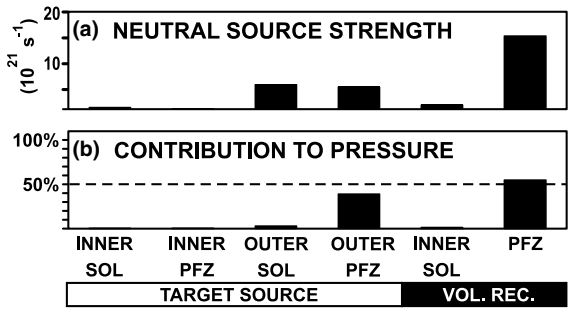

Fig. 7. (a) Neutral source strengths for thee divertor. (b) The percentage of the calculated neutral pressure generated by neutrals from the individual sources.

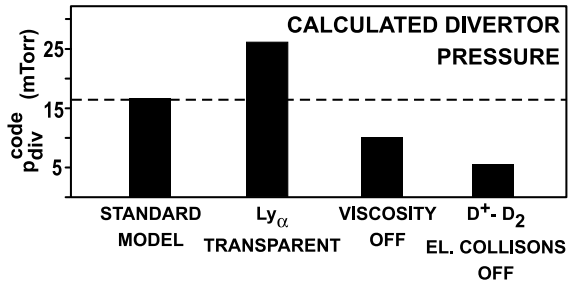

Fig. 8. The change in the calculated neutral pressure when various processes are removed from the neutral model in EIRENE.

3.1. Volume recombination and opacity to Ly_α photons

Radiative, 3-body and molecular assisted recombination [19] (MAR) contribute 1%, 89%, and 10% of the total recombination source, respectively.

The peak atom density in the PFZ is 1.3×10^{20} m^{-3}, and the associated absorption of Ly_α photons can result in a significant steady-state population of excited n_D ($p = 2$) atoms. The ionization potential is lower for the excited atoms (3.4 eV) than for the ground state (13.6 eV), which substantially increases the ionization rate in regions of low T_e, i.e. the PFZ. The loss of the photon from the system when the absorber is ionized before re-emission is referred to as 'trapping'.

If photon transport is *not* included in the neutral model, the calculated divertor pressure increases to ~25 mTorr. For photon transport included, ~90% of the Ly_α photons emitted in the PFZ are trapped, consistent with strong trapping levels observed experimentally [2]. The prompt re-ionisation of atoms due to Ly_α opacity effectively reduces S_{rec} in the PFZ by a factor ~2. The model employed here includes Doppler and natural broadening, and follows Ly_α photons only. Zeeman splitting (in development) will reduce the trapping but this will be offset by the inclusion of additional Lyman lines.

3.2. Neutral viscosity

The neutral molecule density, n_{D_2}, is plotted in Fig. 9(a). The density gradient at the entrance to the plenum is due to: (a) the temperature gradient between higher energy molecules outside the plenum, which have partially thermalized with the plasma via D^+–D_2 elastic collisions, and the colder gas inside the plenum that has thermalized with the walls, and (b) the higher energy neutrals 'pushing' on the colder plenum gas via neutral-neutral collisions. The difference between the radial variation in n_{D_2} through the plenum entrance (white dashed line in Fig. 9(a)) for the viscous and inviscid neutral solutions is shown in Fig. 9(c).

Fig. 9(b) shows the neutral molecule pressure, p_{D_2}. The molecular pressure is 25 mTorr just outside the plenum, but roughly half of the neutral momentum is lost to the wall near the entrance, giving a lower pressure inside the plenum. The radial variation in p_{D_2} is shown in Fig. 9(d) for cases with and without viscosity.

Neutral–plasma interactions dominate outside the plenum and therefore the solution in the divertor proper

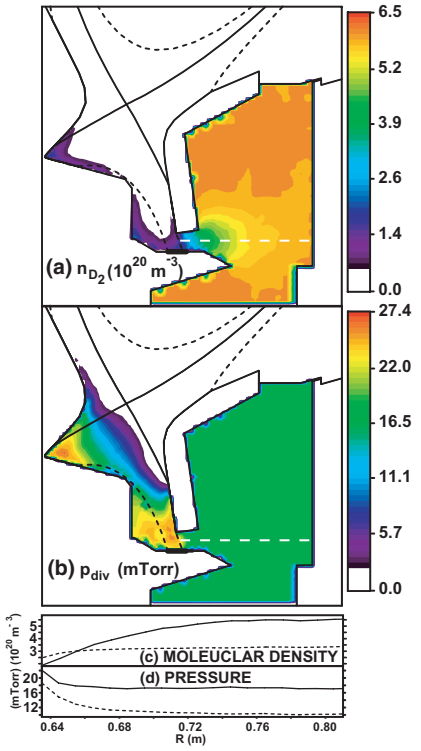

Fig. 9. (a) The neutral molecule density distribution for the standard case (linear scale). (b) The neutral molecule pressure for the standard case (linear scale). (c) Radial variation [along the dashed horizontal line in (a)] of the molecule density with (solid) and without (dashed) viscosity included in the model. (d) Radial pressure variation, as in (c).

is not strongly affected by neutral viscosity, unlike in the plenum.

3.3. D^+–D_2 elastic collisions

Removing elastic collisions between plasma ions and neutral molecules reduces the divertor pressure by a factor 3–4 to 5 mTorr. This strong dependence is a result of the high probability that molecules exiting the plenum will scatter off the cold, dense plasma in the outer PFZ. This is referred to as the *albedo*, A, of the plasma. For a given 'primary influx' of neutrals into the plenum (particles entering for the first time), Φ_0, the total influx, Φ_{tot}, consists of Φ_0 plus the flux of neutrals that exit and then return before they are ionized by the plasma. Φ_{tot} (Φ_0, A) is given by:

$$\Phi_{tot} = \frac{\Phi_0}{1 - A}, \tag{1}$$

which is highly nonlinear as $A \to 1$. For the plasma solution in Section 2.3, A is 0.81 when D^+–D_2 elastic collisions are included and Φ_{tot} is a factor 5 higher than Φ_0. Removing D^+–D_2 gives $A = 0.55$, with A non-zero because neutrals can still return to the plenum after wall collisions or dissociation.

This strong dependence of Φ_{tot} on the D^+–D_2 collision rate for $A \to 1$ suggests that p_{div}^{code} is sensitive to $\sigma_{D^+-D_2}$, and indeed, increasing $\sigma_{D^+-D_2}$ by 50% in the model raises the pressure to 21 mTorr. However, the cross-sections in EIRENE are in agreement with recent quantal calculations [20] with uncertainties reported to be less than 50%.

3.4. Divertor leakage

There are toroidal and poloidal gaps in the C-Mod outer divertor that provide additional leakage pathways for neutrals to escape the plenum. Including these pathways in the model via a 3D representation of the outer divertor in EIRENE [10] reduces p_{div}^{code} to 11 ± 3 mTorr, significantly increasing the discrepancy with the measured pressure. The increase in the relative uncertainty as compared to the sealed plenum result is due to the presence of a poloidal gap between the outer divertor cassettes and the vessel wall, which is filled with loose fitting glass block and therefore poorly characterized in the model. Note that much of the above analysis is still valid since p_{div}^{code} is only lower by 40%, but the 3D result suggests that an important aspect(s) of the C-Mod divertor is still not included in the model.

4. Summary and conclusions

The calculated divertor pressure for 3D EIRENE, which includes all significant leakage pathways from the plenum to the main chamber, was 11 ± 3 mTorr, a factor ~2 lower than the measured pressure of 25 ± 3 mTorr. The result for the 'sealed plenum' approximation is 17 ± 2 mTorr, a factor 5–6 higher than for the previous neutral modeling studies of the C-Mod divertor. The neutral solution was strongly influence by opacity to Ly_α photons, viscosity, and elastic collisions between plasma ions and neutral molecules. Note that the calculated pressures reported here are the first C-Mod results to include the effect of Ly_α trapping, which *reduces* the calculated pressure by ~30%.

The improved agreement with experiment is due to more detailed modeling of detached plasma profiles, in particular the introduction of partially detached plasma in the outer PFZ. The empirical plasma model successfully generates a divertor plasma solution that has broad agreement with the available experimental data, almost within uncertainties. Exceptions are the magnitude of the D_α and D_γ emissions which where high in the model by a factor ~2.

The results indicate that much of the controlling neutral physics for a collisional, ITER-like divertor is well represented in EIRENE. Future work to investigate

the remaining factor ~2 discrepancy with the measured pressure includes a continuing review of the experimental data, refinement of the plasma solution, more complete opacity modeling, an approximation for plasma oscillations, better characterization of the lower divertor (more data), the inclusion of additional charge carriers (H_2^+, H_3^+, H^-) near surfaces in the lower divertor, and the transport of vibrationally excited molecules into the plenum.

Acknowledgment

Thanks for the support of P.C. Stangeby, and also D. Reiter who offered a great deal of helpful suggestions. This work was supported by US DOE Contract No. DE-AC02-78ET51013 and the National Sciences and Engineering Research Council of Canada.

References

[1] D.B. Heifitz, Physics of Plasma Wall Interaction in Controlled Fusions, Plenum, Oxford, 1986, p. 695.
[2] J.L. Terry et al., Phys. Plasmas 5 (5) (1998) 1759.
[3] D. Reiter, The EIRENE Code. http://www.eirene.de.
[4] D.P. Stotler, C.F.F. Karney, Contrib. Plasma Phys. 34 (1994) 392.
[5] I.H. Hutchinson et al., Phys. Plasmas 1 (5) (1994) 1511.
[6] A. Niemczewski et al., Nucl. Fusion 37 (2) (1997) 151.
[7] D.P. Stotler et al., J. Nucl. Mater. 290–293 (2001) 967.
[8] J.D. Elder et al. 2000 APS poster. http://starfire.utias.utoronto.ca/DIVIMP/publications.
[9] D.P. Stotler et al., PPPL Report 3690 (2002).
[10] S. Lisgo, Ph.D. Thesis, U. Toronto, http://starfire.utias.utoronto.ca/DIVIMP/publications.
[11] D.E. Post, J. Nucl. Mater. 220–222 (1995) 143.
[12] P.C. Stangeby, The Plasma Boundary of Magnetic Fusion Devices, Institute of Physics, Bristol, 2002.
[13] S. Lisgo, P.C. Stangeby et al., these Proceedings. doi:10.1016/j.jnucmat.2004.09.055.
[14] P.C. Stangeby, J.D. Elder, A Guide to the DIVIMP Code. http://starfire.utias.utoronto.ca.
[15] B. Lipschultz et al., Phys. Plasmas 6 (5) (1999) 1907.
[16] B. LaBombard et al., J. Nucl. Mater. 220–222 (1995) 976.
[17] G. Fussmann et al., J. Nucl. Mater. 128&129 (1984) 350.
[18] E.M. Hollmann et al., Rev. Sci. Instrum. 74 (9) (2003) 3984.
[19] U. Fantz et al., J. Nucl. Mater. 290–293 (2001) 367.
[20] P.S. Krstic, D.R. Schultz, Atomic and Plasma Material-Interaction Data for Fusion, Volume 8, Vienna: IAEA, 1998.